Journal of Materials Science & Technology 34 (2018) 1544–1549

Contents lists available at ScienceDirect

Journal of Materials Science & Technology

journal homepage: www.jmst.org

Solvothermal-assisted morphology evolution of nanostructured $LiMnPO_4$ as high-performance lithium-ion batteries cathode

Chongjia Zhu [a], Zhiqiu Wu [a], Jian Xie [a,b,*], Zhen Chen [c], Jian Tu [c], Gaoshao Cao [b,**], Xinbing Zhao [a,b]

[a] State Key Laboratory of Silicon Materials, School of Materials Science and Engineering, Zhejiang University, Hangzhou 310027, China
[b] Key Laboratory of Advanced Materials and Applications for Batteries of Zhejiang Province, Hangzhou 310027, China
[c] LI-FUN Technology Corporation Limited, Zhuzhou 412000, China

ARTICLE INFO

Article history:
Received 22 December 2017
Received in revised form 11 January 2018
Accepted 29 March 2018
Available online 23 April 2018

Keywords:
Lithium manganese phosphate
Cathode
Solvothermal reaction
Lithium-ion battery
Electrochemical performance

ABSTRACT

As a potential substitute for $LiFePO_4$, $LiMnPO_4$ has attracted more and more attention due to its higher energy, showing potential application in electric vehicle (EV) or hybrid electric vehicle (HEV). In this work, solvothermal method was used to prepare nano-sized $LiMnPO_4$, where ethylene glycol was used as solvent, and lithium acetate (LiAc), phosphoric acid (H_3PO_4) and manganese chloride ($MnCl_2$) were used as precursors. The crystal structure and morphology of the obtained products were characterized by X-ray diffraction, scanning electron microscopy and transmission electron microscopy. The electrochemical performance was evaluated by charge-discharge cycling, cyclic voltammetry and electrochemical impedance spectroscopy. The results show that the molar ratio of LiAc:H_3PO_4:$MnCl_2$ plays a critical role in directing the morphology of $LiMnPO_4$. Large plates transform into irregular nanoparticles when the molar ratio changes from 2:1:1 to 6:1:1. After carbon coating, the product prepared from the 6:1:1 precursor could deliver discharge capacities of 156.9, 122.8, and 89.7 mAh g^{-1} at 0.05C, 1C and 10C, respectively. The capacity retention can be maintained at 85.1% after 200 cycles at 1C rate for this product.

1. Introduction

The discovery of $LiFePO_4$ opened the research history of olivine-type cathode materials for lithium-ion batteries [1]. The successful commercialization of $LiFePO_4$ for electric vehicle (EV) or hybrid electric vehicle (HEV) is attributed to its low cost, environmental friendliness, good chemical/electrochemical stability, and high safety [2–5]. Besides, the olivine-type phosphate has a moderate theoretical capacity of 170 mAh g^{-1}. Compared with $LiFePO_4$, $LiMnPO_4$ is a more promising cathode with higher energy density due to its higher Mn^{2+}/Mn^{3+} redox potential (4.1 V vs. Li/Li^+) than that of $LiFePO_4$ (3.45 V) [6].

However, $LiMnPO_4$ shows much poorer electrochemical performance than $LiFePO_4$ although the two materials have a same crystal structure. There are some factors that limit the electrochemical activity of $LiMnPO_4$: low electronic conductivity ($<10^{-12}$ S cm^{-1}) [7], low lithium-ion diffusion rate ($<10^{-16}$–10^{-14} cm^2 s^{-1}), Jahn-Teller lattice distortion in Mn^{3+}, the interface strain between the $LiMnPO_4$ and $MnPO_4$ phases, and metastability of the $MnPO_4$ phase [8]. Particle size or morphology control, surface modification [9] and supervalent ion doping [10] are three main strategies to overcome these limitations. Solvothermal route is widely used to prepare nanometer materials of olivine-type phosphates. For the solvothermal synthesis, the morphology and electrochemical performance of the $LiMnPO_4$ are determined by many factors such as precursortypes [11], charging sequence [12], use of additives or surfactants [13–17], pH [18,19], and solvent types [20].

Previous work has shown that $LiMnPO_4$ with different orientations [21] or morphologies including spindles [22], dumbbells [23,24], balls [25,26], flowers [27–29], plates [30], and rods [31] has been prepared by adjusting the molar ratio and pH of the precursors. Generally, a nanostructure is necessary to obtain high performance of $LiMnPO_4$. However, the synthesis of nanostructured $LiMnPO_4$ with a facile route has been rarely reported to date. In this work, we proposed a facile method to decrease the particle size of $LiMnPO_4$ to nanoscale by simply adjusting the molar ratio of the precursors. In doing so, the electrochemical activity of $LiMnPO_4$

* Corresponding author at: State Key Laboratory of Silicon Materials, School of Materials Science and Engineering, Zhejiang University, Hangzhou 310027, China.
** Corresponding author.
E-mail addresses: xiejian1977@zju.edu.cn (J. Xie), gscao@zju.edu.cn (G. Cao).

https://doi.org/10.1016/j.jmst.2018.04.017
1005-0302/

was enhanced, leading to high capacity, excellent rate capability and long cycle life.

2. Experimental

The reagents include lithium acetate dehydrate (LiAc·$2H_2O$, Analytical reagent (AR) grade), phosphoric acid (H_3PO_4, 85 wt%), manganese chloridetetrahydrate ($MnCl_2·4H_2O$, AR grade), glucose (AR grade) and ethylene glycol (EG). $LiMnPO_4$ was synthesized by a facile one-step solvothermal route via the reaction $H_3PO_4 + 3LiAc + MnCl_2 \rightarrow LiMnPO_4 + 2LiCl + 3HAc$. First, $12x$ mmol of LiAc·$2H_2O$ (x = 2, 2.5, 3, 4, 5, 6) was dissolved in 30 mL of EG. Then, 820 μL (12 mmol) of H_3PO_4 was added dropwise to the above solution to form a suspension. After vigorous stirring for 10 min, a solution of 12 mmol $MnCl_2·4H_2O$ in 30 mL EG was added dropwise into the above suspension. After stirring for another 10 min, the suspension was sealed in an 80 mL Teflon-lined stainless steel autoclave. The autoclave was then heated at 180 °C for 10 h in an electric oven followed by cooling to room temperature naturally. The as-obtained white precipitate was separated by centrifugation at a speed of 12000 rpm, washed with deionized (DI) water and ethanol for three times, and dried at 80 °C for 12 h in vacuum. The $LiMnPO_4$ samples synthesized with different x values are named LMP-x. To prepare carbon-coated $LiMnPO_4$ ($LiMnPO_4$/C), 1 g of $LiMnPO_4$ powder was mixed with 0.5 g of glucose in 3 mL of DI water. The mixture was ultrasonically dispersed for 1 h and the water was evaporated by heating at 80 °C in air. After being grounded in a mortar, the dried powder was heated to 600 °C at 5 °C min^{-1} in a tube furnace and held for 4 h under Ar atmosphere. For simplicity, the names of the carbon-coated samples are same as the pristine ones.

The crystal structure and phase purity of the products were determined by X-ray diffraction (XRD) on a Rigaku D/Max 2550 pc powder diffractometer using CuK_α radiation (wavelength = 0.1541 nm). The morphology of the samples was identified by scanning electron microscopy (SEM) on an S-4800 field emission scanning electron microscope (Hitachi, Japan). The microstructures were observed by transmission electron microscopy (TEM), high-resolution TEM (HRTEM) and selected area electron diffraction (SAED) on an FEI Tecnai G^2 F20S-Twin high-resolution transmission electron microscope with an acceleration voltage of 200 kV. The amount of the coated carbon in $LiMnPO_4$/C was measured on a Flash EA 1112 tester.

The electrode slurry was fabricated by mixing 70 wt% $LiMnPO_4$/C active material, 20 wt% acetylene black and 10 wt% poly(vinyldifluoride) binder in N-methylpyrrolidone with magnetic stirring. The slurry was uniformly coated onto polished aluminum foils, followed by drying in vacuum at 110 °C overnight to form working electrodes. The loading of the active material in electrode is about 2 mg cm^{-2}. The electrodes were pressed at 10 MPa before cell assembly. CR2025 coin-type cells were assembled in an argon-filled glove box using Celgard 2300 membrane as separators and lithium foils as counter electrodes. 1 mol L^{-1} $LiPF_6$ in ethylene carbonate (EC)/dimethyl carbonate (DMC) (1:1 in volume) was used as electrolyte. The cells were tested using a constant-current-constant-voltage (CC-CV) mode between 2.0-4.5 V (vs. Li/Li^+) on a Neware BTS-5V–10 mA battery cycler (Shenzhen, China). The cells were charged at different current rates to 4.5 V, then held at 4.5 V until the current decreases to 0.01C (current rate 1C = 170 mA g^{-1}), and finally discharged to 2.0 V at the same current rate. The charge rate was the same as the discharge rate for all the tests. Cyclic voltammetry (CV) scanning was performed on a CHI660C electrochemistry work station in the voltage range of 3.0–4.8 V (vs. Li/Li^+) at various scan rates. Electrochemical impedance spectroscopy (EIS) measurements were conducted by applying an alternative current voltage of 5 mV amplitude in the frequency range from 10 mHz to 100 kHz on the electrochemistry work station. All of the electrochemical measurements were carried out at room temperature (25 °C).

3. Results and discussion

The crystal structure of olivine-type $LiMnPO_4$ perpendicular to the b axis and the lithium-ion diffusion pathway are shown in Fig. 1. The zigzag one-dimensional diffusion tunnels of Li ions along the b axis was verified by theoretical calculation [32] and experimental visualization [33]. The structure consists of a distorted hexagonal close-packed (hcp) oxygen framework. Li and Mn atoms are located in 1/2 of octahedral holes and P occupies 1/8 of the tetrahedral holes. This crystal structure results in rather low electronic conductivity and lithium-ion diffusion rate and thus poor electrochemical performance of $LiMnPO_4$.

Fig. 2 shows the XRD patterns of the as-synthesized $LiMnPO_4$ and $LiMnPO_4$/C. For all the LMP-x samples, the diffraction peaks can be indexed to an orthorhombic structure with a *Pnma* space group (JCPDS No. 74-0375). Although a minor $Mn_7(PO_3OH)_4(PO_4)_2$ phase is found in LMP-2 sample, it disappears after the carbon-coating step. It is expected that the carbon-coating process would enhance the crystallization of $LiMnPO_4$, besides the contribution to the electronic conductivity.

Fig. 3 shows the SEM images of $LiMnPO_4$ prepared with different molar ratios of the precursors. It is noted that the morphologies of the samples depend on the molar ratio of LiAc, H_3PO_4 and $MnCl_2$. The size of $LiMnPO_4$ particles tends to decrease with the increase in LiAc amount. LMP-2 sample consists of irregular plates with a length of around 500 nm and a thickness of 20 nm. For LMP-2.5, two shapes of plates and particles coexist, but the size of the plates is reduced to about 300 nm in length. For LMP-3, the size of the plates is further reduced to around 200 nm and more nanoparticles below 100 nm appear. All the plates transform to nanoparticles when the x value exceeds 4. At this x value, the size of the nanoparticles is below 100 nm as seen in Fig. 3(d)–(f). Further increasing the x value does not decrease the particle size of $LiMnPO_4$ obviously.

Fig. 4 shows the typical TEM image of LMP-5 after carbon coating. It can be seen that the particle size is smaller than 100 nm, agreeing with the SEM observation. It is noted that the size of some particles is as small as 20 nm, which is favorable for rapid lithium-ion transport. HRTEM image indicates that the $LiMnPO_4$ sample is well crystallized after the carbon-coating step. The lattice spacing of 0.4276 nm corresponds to (101) plane of $LiMnPO_4$. As shown in Fig. 4, a thin amorphous carbon layer of around 2 nm thickness can be observed on the surface of $LiMnPO_4$. The thin carbon layer is desirable for barrier-free lithium-ion diffusion. In addition, the carbon layer is uniform which is critical in increasing the electronic conductivity. The carbon contents of the above mentioned six samples are 9.0%, 12.2%, 11.0%, 10.1%, 10.9% and 10.8%, respectively.

The discharge profiles of the carbon-coated samples at different rates are shown in Fig. 5. For the rate capability tests, a CC-CV mode was applied at various current rates from 0.05C to 20C with 5 cycles at each current density. All the samples have a discharge plateau at around 4.1 V vs. Li/Li^+. For LMP-2, its initial discharge capacity at 0.05C is only 39.3 mAh g^{-1} indicating low electrochemical activity as seen in Fig. 5(a). Sample LMP-2.5 exhibits a much higher discharge capacity than LMP-2, but its capacity decreases rapidly to 34.9 mAh g^{-1} at 20C, suggesting poor rate capability in Fig. 5(b). The rate capability of LMP-3 is slightly enhanced compared with LMP-2 and LMP-2.5 in Fig. 5(c). Clearly, the enhanced rate capability is closely related to the decrease in particle size since these samples have a similar carbon content. LMP-4 can deliver a discharge capacity of 156.8 mAh g^{-1} at 0.05C, much higher than those of the

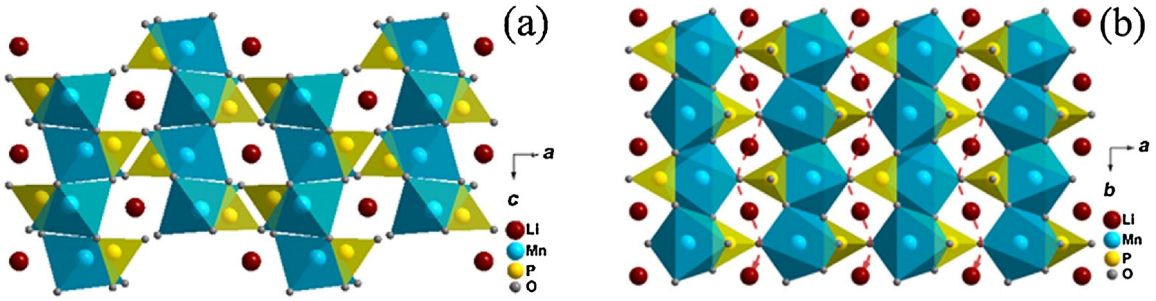

Fig. 1. (a) Crystal structure of olivine-type $LiMnPO_4$ projected along the [010] and (b) lithium-ion diffusion pathway parallel to [010].

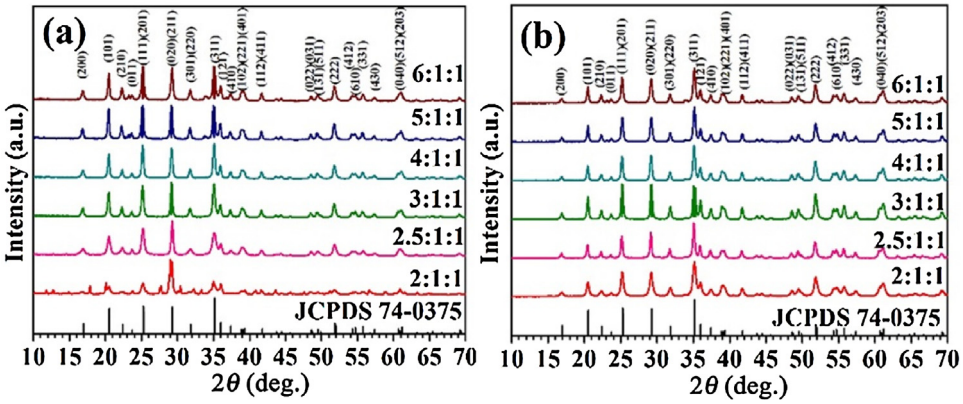

Fig. 2. XRD patterns of (a) $LiMnPO_4$ and (b) $LiMnPO_4$/C.

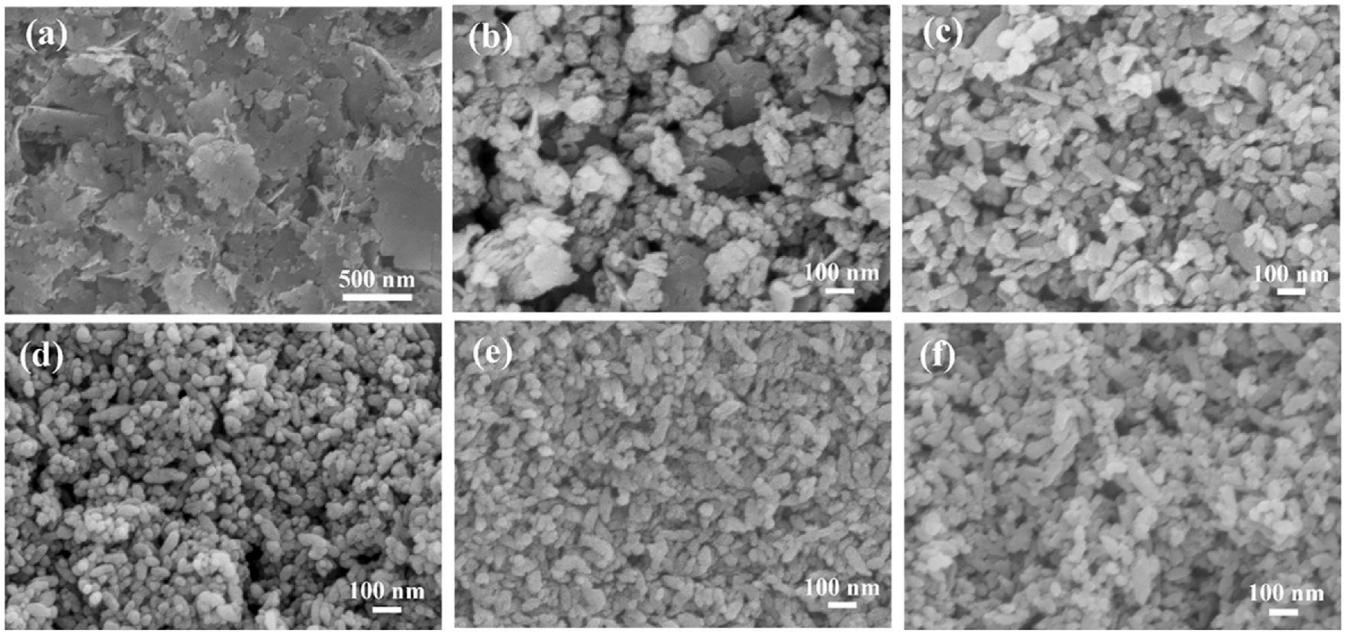

Fig. 3. SEM images of as-obtained $LiMnPO_4$: (a) LMP-2; (b) LMP-2.5; (c) LMP-3; (d) LMP-4; (e) LMP-5; (f) LMP-6.

above samples, indicating the considerably improved electrochemical activity in Fig. 5(d). The discharge capacities of LMP-5 in Fig. 5(e) are 157.3, 151.9, 133.1, 124.1, 114.1, 99.2, 87.4 and 71.7 mAh g^{-1} at 0.05C, 0.1C, 0.5C, 1C, 2C, 5C, 10C and 20C, respectively. The discharge capacity of LMP-6 is close to that of LMP-5 as shown in Fig. 5(f). The difference in rate capability among these samples is compared in Fig. 5(g) and (h). Clearly, the rate capability of these samples is strongly dependent on their size and morphology. It suggests that increasing LiAc ratio in the precursor can enhance the rate capability of $LiMnPO_4$/C by decreasing the size of $LiMnPO_4$.

The cycling performance of $LiMnPO_4$/C at current rates of 1C and 5C is shown in Fig. 6. Although LMP-2.5 and LMP-3 can show a stable cycling at 1C, their capacities are low (below 90 mAh g^{-1}), indicating low electrochemical activity of the materials due to a large particle size. In contrast, LMP-4, LMP-5 and LMP-6 can deliver high initial capacities close to 120 mAh g^{-1}. Among the above three

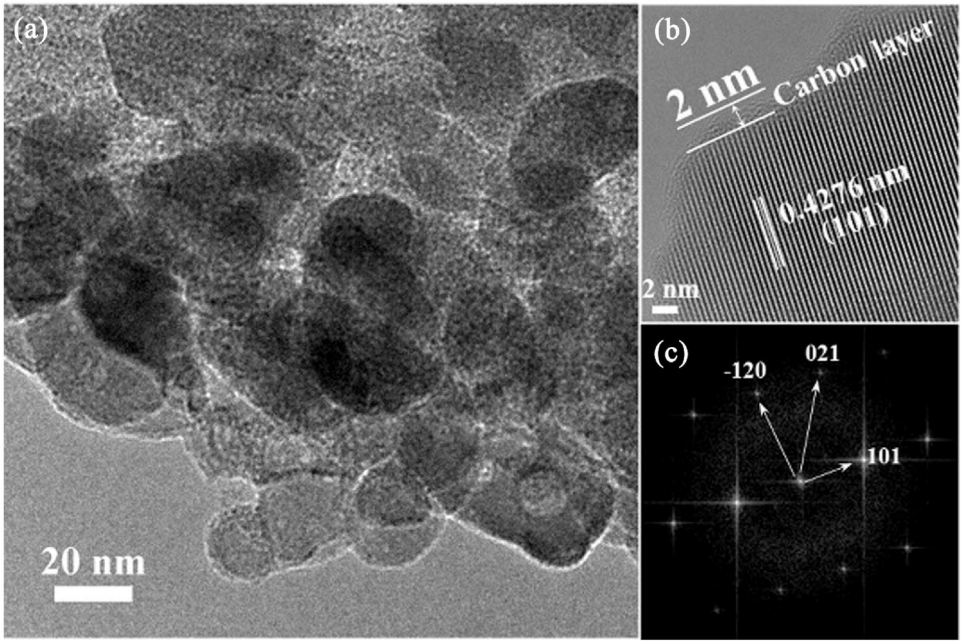

Fig. 4. (a) TEM, (b) HRTEM images and (c) SAED pattern of carbon-coated LMP-5.

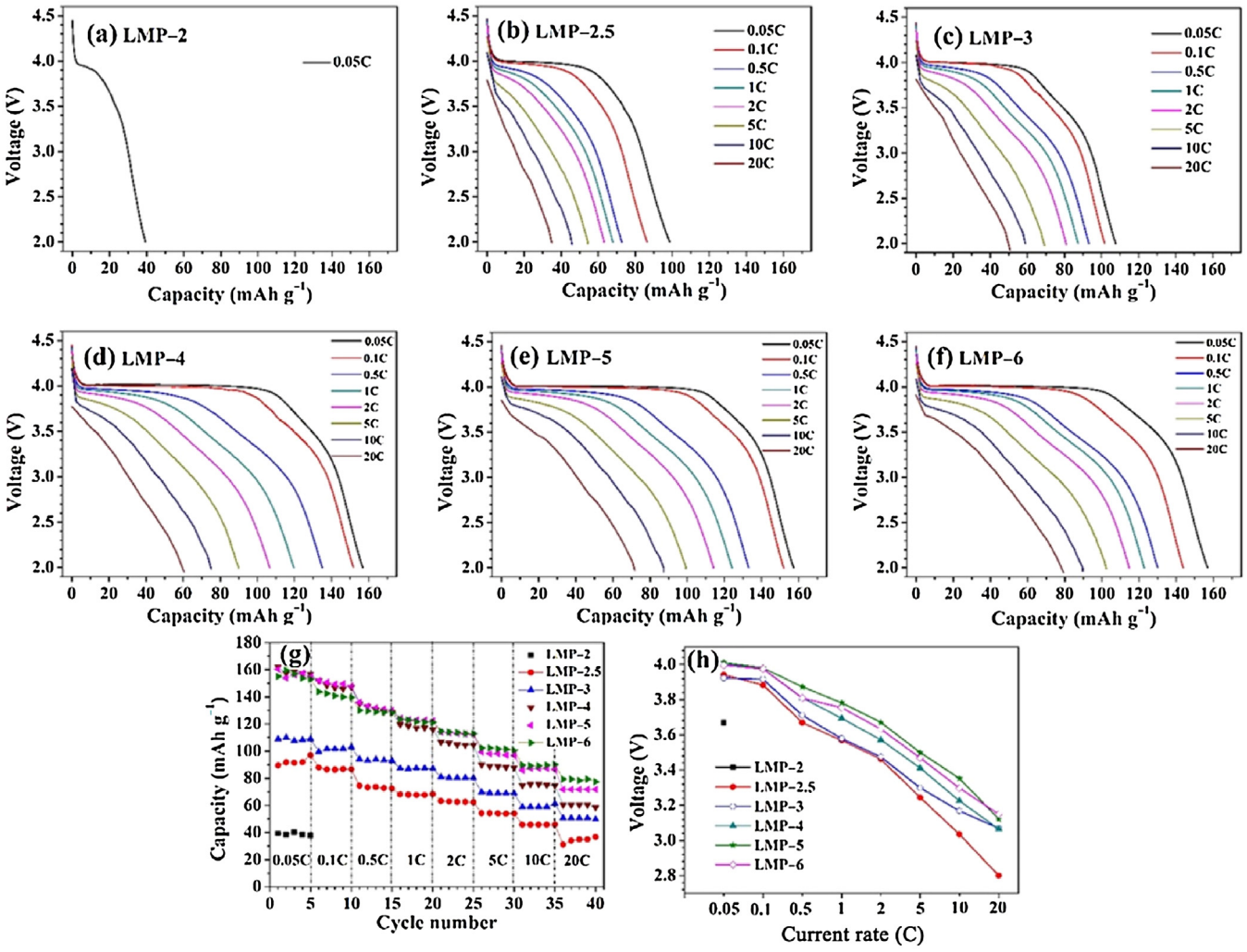

Fig. 5. Discharge profiles of (a) LMP-2, (b) LMP-2.5, (c) LMP-3, (d) LMP-4, (e) LMP-5, (f) LMP-6, (g) rate performance of LMP-*x* and (h) median voltage (voltage at half of discharge capacity) vs. current rate.

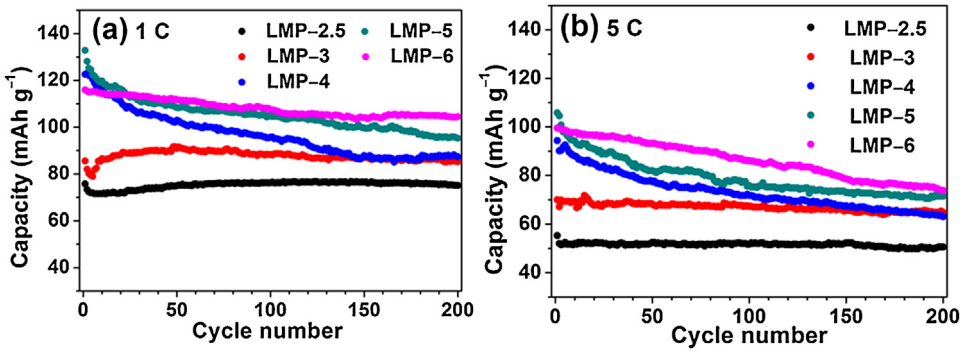

Fig. 6. Cycling performance of carbon-coated LMP-*x* at (a) 1C and (b) 5C.

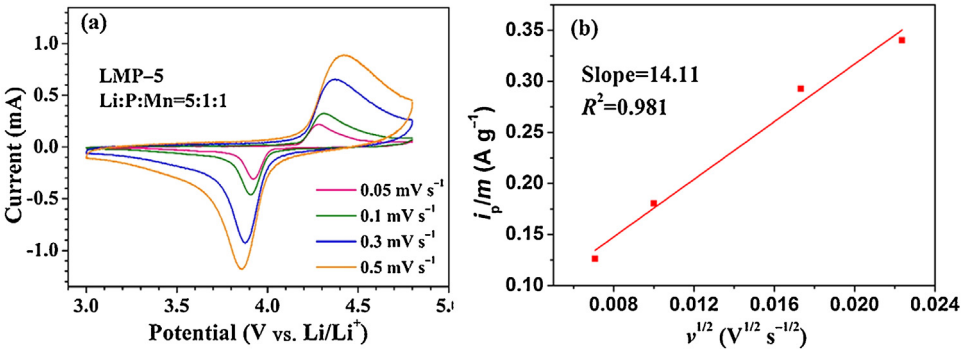

Fig. 7. (a) CV plots of LMP-5 and (b) linear response of cathodic peak current density as a function of square root of scan rate (*R*: goodness of fit; *m*: weight of active material on the electrode).

samples, LMP-6 exhibits the best cycling stability with a capacity retention of 85.1% after 200 cycles. Even at 5C, LMP-6 can keep more than 70% of its initial capacity after 200 cycles, indicative of superior high-rate cycling stability. The excellent cycling stability at high rates can be attributed to its small particle size with reduced lattice strain during lithiation/delithiation and uniform carbon coating.

CV scanning of LMP-5 sample was performed at various rates in the voltage range of 3.0–4.8 V to investigate the lithium-ion diffusion kinetics. Fig. 7 shows the CV plots and the corresponding linear fitting. Randles-Sevcik equation is used to calculate the lithium-ion chemical diffusion coefficient of LMP-5:

$$i_p = 2.69 \times 10^5 n^{3/2} C_{Li} A D^{1/2} v^{1/2} \quad (1)$$

where i_p is the peak current density at different scan rates ($A\,g^{-1}$), n is the number of electrons involved in the redox process ($n = 1$ for the Mn^{2+}/Mn^{3+} redox pair), C_{Li} is the initial concentration of lithium ions in $LiMnPO_4$ (0.0223 mol cm^{-3}), A is the contact area ($cm^2\,g^{-1}$) between the electrolyte and the activematerials (corresponding to the BET specific surface area), D is the lithium-ion diffusion coefficient ($cm^2\,s^{-1}$), and v is the scan rate ($V\,s^{-1}$). The Brunauer-Emmett-Teller (BET) specific area of LMP-5 is 48.4 $m^2\,g^{-1}$. The lithium-ion diffusion coefficient of LMP-5 was calculated to be 1.6×10^{-17} $cm^2\,s^{-1}$. Despite the intrinsic low lithium-ion diffusion rate, the material still displays superior rate capability due to its small particle size.

EIS measurements were performed after 5 cycles at 0.05C to further reveal the difference in the electrochemical activity of the six $LiMnPO_4$/C composites as shown in Fig. 8. All the EIS plots include a semicircle in the high-medium frequency region and a straight line in the low frequency regionin Fig. 8(a). The plots are fitted using an equivalent circuit shown in Fig. 8(b). The intercept at Z' axis corresponds to the ohmic resistance (R_e), which includes the total resistance of particle-particle contact resistance, electrolyte resistance and electrolyte-current collector interface resistance. The

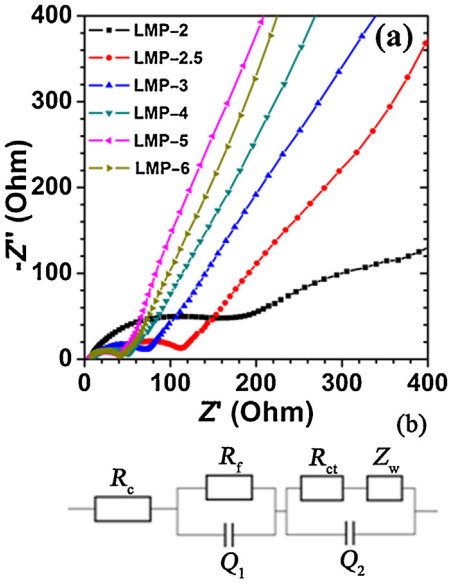

Fig. 8. (a) EIS plots of cells after 5 cycles at 0.05C and (b) corresponding equivalent circuit.

dimension of the depressed semicircles corresponds to the charge transfer resistance (R_{ct}) at electrode/electrolyte interface and the double-layer capacitance between the electrolyte and cathode [14]. The inclined line is attributed to Warburg impedance associated with the diffusion of lithium-ions in the bulk material. It is noted that reducing the particle size of $LiMnPO_4$ generally decreases the charge transfer resistance. This can explain the outstanding rate capability and high-rate cycling stability of the small-sized $LiMnPO_4$/C. As seen in Fig. 9, the rate performance of our sample is among the best ones reported so far [12,18–20,34–37].

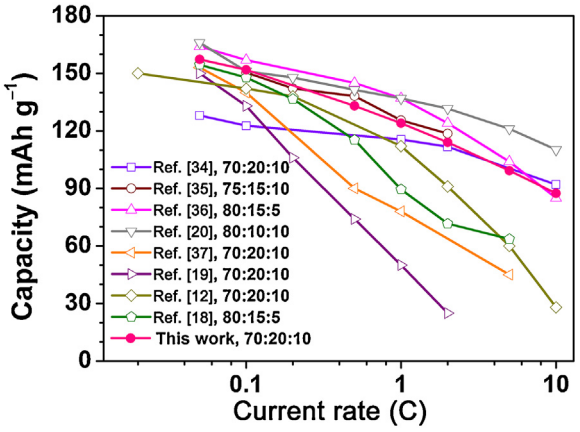

Fig. 9. Comparison of rate capability of sample and some typical $LiMnPO_4$/C materials reported previously. The inset gives the $LiMnPO_4$/conductive carbon/binder weight ratio.

4. Conclusion

In summary, we synthesized $LiMnPO_4$ nanoparticles by a simple solvothermal method. The results show that the morphology of $LiMnPO_4$ is dependent on the LiAc:H_3PO_4:$MnCl_2$ molar ratio. At low ratios, the $LiMnPO_4$ has an irregular plate shape with a size of around 500 nm, which exhibits poor electrochemical performance. At high ratios, the plates change into nanoparticles of around 100 nm. When molar ratio of LiAc/H_3PO_4/$MnCl_2$ is 6:1:1 in the precursor, the product after carbon coating yields the highest discharge capacities of 156.9, 122.8, 89.7 mAh g^{-1} at 0.05C, 1C and 10C. After 200 cycles at currenet rate of 1C, it can retain 85% of its initial capacity. This work provides a facile method to prepare small-sized $LiMnPO_4$ with superior rate capability and high-rate cycling stability by simply adjusting the molar ratios of the starting materials.

Acknowledgements

This work was supported financially by the National Natural Science Foundation of China (No. 51572238) and the Strategic Emerging Industry Project of Hunan Province, China (No. 2016GK4030).

References

[1] A.K. Padhi, K.S. Nanjundaswamy, J.B. Goodenough, J. Electrochem. Soc. 144 (1997) 1188–1194.
[2] N. Mahmood, Y. Hou, Adv. Sci. 1 (2014) 1400012.
[3] V. Aravindan, J. Gnanaraj, Y.S. Lee, S. Madhavi, J. Mater. Chem. A 1 (2013) 3518–3539.
[4] J. Kim, D.H. Seo, S.W. Kim, Y.U. Park, K. Kang, Chem. Commun. 46 (2010) 1305–1307.
[5] A. Manthiram, A.V. Murugan, A. Sarkar, T. Muraliganth, Energy Environ. Sci. 1 (2008) 621–638.
[6] M.K. Devaraju, I. Honma, Adv. Energy Mater. 2 (2012) 284–297.
[7] M.S. Kim, J.P. Jegal, K.C. Roh, K.B. Kim, J. Mater. Chem. A 2 (2014) 10607–10613.
[8] P. Nie, L. Shen, F. Zhang, L. Chen, H. Deng, X. Zhang, CrystEngComm 14 (2012) 4284–4288.
[9] S. Liu, H. Fang, E. Dai, B. Yang, Y. Yao, W. Ma, Y. Dai, Electrochim. Acta 116 (2014) 97–102.
[10] C. Hu, H. Yi, H. Fang, B. Yang, Y. Yao, W. Ma, Y. Dai, Electrochem. Commun. 12 (2010) 1784–1787.
[11] F. Zhou, P. Zhu, X. Fu, R. Chen, R. Sun, C.P. Wong, CrystEngComm 16 (2014) 766–774.
[12] T.H. Kim, H.S. Park, M.H. Lee, S.Y. Lee, H.K. Song, J. Power Sources 210 (2012) 1–6.
[13] W. Zhang, Z. Shan, K. Zhu, S. Liu, X. Liu, J. Tian, Electrochim. Acta 153 (2015) 385–392.
[14] X. Zhou, Y. Deng, L. Wan, X. Qin, G. Chen, J. Power Sources 265 (2014) 223–230.
[15] H.C. Dinh, S.I. Mho, Y. Kang, I.H. Yeo, J. Power Sources 244 (2013) 189–195.
[16] F. Wang, J. Yang, P. Gao, Y.N. Li, J. Wang, J. Power Sources 196 (2011) 10258–10262.
[17] Y. Wang, Y. Yang, Y. Yang, H. Shao, Solid State Commun. 150 (2010) 81–85.
[18] Z. Qin, X. Zhou, Y. Xia, C. Tang, Z. Liu, J. Mater. Chem. 22 (2012) 21144–21153.
[19] S.L. Yang, R.G. Ma, M.J. Hu, L.J. Xi, Z.G. Lu, C.Y. Chung, J. Mater. Chem. 22 (2012) 25402–25408.
[20] Y. Hong, Z. Tang, S. Wang, W. Quan, Z. Zhang, J. Mater. Chem. A 3 (2015) 10267–10274.
[21] H. Guo, C. Wu, J. Xie, S. Zhang, G. Cao, X. Zhao, J. Mater. Chem. A 2 (2014) 10581–10588.
[22] Y. Xia, W. Zhang, H. Huang, Y. Gan, J. Tian, X. Tao, J. Power Sources 196 (2011) 5651–5658.
[23] B. Guo, H. Ruan, C. Zheng, H. Fei, M. Wei, Sci. Rep. 3 (2013) 2788.
[24] N. Zhou, H.Y. Wang, E. Uchaker, M. Zhang, S.Q. Liu, Y.N. Liu, G. Cao, J. Power Sources 239 (2013) 103–110.
[25] M.Y. Cho, H. Kim, H. Kim, Y.S. Lim, K.B. Kim, J.W. Lee, K. Kang, K.C. Roh, J. Mater. Chem. A 2 (2014) 5922–5927.
[26] M.H. Lee, J.Y. Kim, H.K. Song, Chem. Commun. 46 (2010) 6795–6797.
[27] D. Chen, W. Wei, R. Wang, X.F. Lang, Y. Tian, L. Guo, Dalton Trans. 41 (2012) 8822–8828.
[28] P.R. Kumar, M. Venkateswarlu, N. Satyanarayana, J. Appl. Electrochem. 42 (2012) 163–167.
[29] D. Rangappa, K. Sone, T. Kudo, I. Honma, J. Power Sources 195 (2010) 6167–6171.
[30] A. Paolella, G. Bertoni, S. Marras, E. Dilena, M. Colombo, M. Prato, A. Riedinger, M. Povia, A. Ansaldo, K. Zaghib, L. Manna, C. George, Nano Lett. 14 (2014) 6828–6835.
[31] Y. Hong, Z. Tang, Z. Hong, Z. Zhang, J. Power Sources 248 (2014) 655–659.
[32] D. Morgan, A. Van der Ven, G. Ceder, Electrochem. Solid State Lett. 7 (2004) A30–A32.
[33] S.I. Nishimura, G. Kobayashi, K. Ohoyama, R. Kanno, M. Yashima, A. Yamada, Nat. Mater. 7 (2008) 707–711.
[34] K.S. Lee, K.J. Lee, Y.S. Kang, T.J. Shin, Y.E. Sung, D. Ahn, Nanoscale 7 (2015) 13860–13867.
[35] Z. Zhang, G. Hu, Y. Cao, J. Duan, K. Du, Z. Peng, RSC Adv. 5 (2015) 81461–81467.
[36] H.C. Dinh, S.I. Mho, I.H. Yeo, Y. Kang, D.W. Kim, RSC Adv. 5 (2015) 100709–100714.
[37] Z. Bakenov, I. Taniguchi, Electrochem. Commun. 12 (2010) 75–78.